Generation of propagating spin waves from edges of magnetic nanostructures pumped by uniform microwave magnetic field

C. S. Davies and V. V. Kruglyak

School of Physics, University of Exeter, Exeter, EX4 4QL, United Kingdom

Thin-film patterned magnetic nanostructures are widely employed within perceived magnonic device architectures to guide and / or manipulate spin waves for data processing and communication purposes. Here, using micromagnetic simulations, we explore how the internal magnetic field non-uniformity inherent to patterned magnetic nanostructures can also be exploited to create spin-wave sources. The spin-wave emission is achieved through the resonant excitation of finite sized regions of increased effective magnetic field formed near the edges of patterned structures. The phenomenon is rather universal and could be used to generate magneto-dipole, dipole-exchange and exchange dominated spin waves. Depending on the frequency of excitation and parameters of the nanostructures the emitted spin waves may form either highly-directional spin-wave caustic beams or more regular plane spin waves.

***Index Terms* — magnonics, antidot, spin waves, demagnetizing field, resonance**

I. Introduction

THE PATTERNING of magnetic nanostructures, in order to steer [1]-[3], modulate [4],[5], or otherwise modify [6],[7] the properties of propagating spin waves, has led to the successful design of many elements of perceived magnonic computing architecture [8]-[12]. Indeed, it has been predicted [13] that this progress could eventually lead to the use of spin waves as information carriers within future data processing and communication technologies.

The patterning, however, is not only capable of modifying the character of propagating and standing spin waves but can also lead to the formation of spin-wave sources. Recently, we demonstrated [14] that an isolated magnetic antidot patterned in an otherwise continuous magnetized film of Yttrium-Iron-Garnet (YIG) creates regions of increased (both static and dynamic) demagnetizing field in its vicinity, relative to that in the continuous film. As a result, upon exciting the whole sample with a microwave magnetic field tuned in frequency so as to resonantly couple [15] only to the regions of the increased demagnetizing field, the latter regions acted as emitters of propagating spin waves.

In Ref. [14], the relatively large thickness of the YIG film (10 μm) and the macroscopic diameter of the antidot (100 μm) led to the magneto-dipole interaction dominating the observed magnetization dynamics. So, the spin waves observed in Ref. [14] formed spin-wave caustic beams [16]. It is well-known however that the magneto-dipole interaction only dominates at the long-wavelength limit. When the system's dimensions instead approach the nanometer scale, the isotropic exchange interaction becomes increasingly important, and must therefore be considered on equal footing. This raises the question of how the character of spin waves excited using the method from Ref. [14] changes upon down-sizing the sample.

Here, we use micromagnetic calculations to investigate how the character of the spin waves excited via the resonant pumping of internal field non-uniformities changes upon the downscaling of the magnonic system. First, we consider spin-waves emitted by circular antidots patterned in 40 nm and 6 nm thick Permalloy-like films. Due to the interplay between the anisotropic magneto-dipole and isotropic exchange interactions, this difference in the film thickness is observed to lead to a dramatic change in the character of the emitted propagating spin waves. In the former (thicker) sample, the propagation of spin waves is highly anisotropic, with a tendency to form caustic beams, whereas in the latter (thinner) sample, a more isotropic spin-wave emission is observed. Finally, we consider a 40 nm thick semi-infinite film (modeled as a very wide stripe) magnetized along its edge. This patterning geometry removes entirely the static contribution of the demagnetizing field. The edge of the stripe is observed to emit propagating spin waves, which is due to the resonant pumping of the regions of increased dynamic demagnetizing field near the edge.

Manuscript received November 5, 2015. Corresponding author: C. S. Davies (e-mail: csd203@exeter.ac.uk).
Digital Object Identifier inserted by IEEE

II. Methodology

Throughout this paper, we use the Object-Oriented Micro-Magnetic Framework (OOMMF) [17] to perform micromagnetic calculations [3]. The antidot samples considered are shown schematically in Fig. 1 (a). A circular antidot of 200 nm diameter is formed within an otherwise continuous film of Permalloy-like material. The exchange stiffness A, magnetization of saturation M_S, gyromagnetic ratio $\gamma/2\pi$ and damping parameter are set to 1.3 μerg/cm, 800 G, 2.80 MHz/Oe and 0.008, respectively. The film thickness s was set to either 40 nm or 6 nm, and a bias field $\boldsymbol{H}_B$ was applied in the plane of the film, parallel to the z-axis. Two-dimensional periodic boundary conditions [18] were applied to a square supercell of 6 μm length (Fig. 1 (a)). As in Ref. [14], the large size of the supercell allowed us to assume the antidot was in isolation. The sample was discretized into 5×5 nm^2 mesh cells in the YZ plane, with no discretization across the sample thickness.

In the first series of simulations, the system was magnetized fully along the z-axis and then relaxed in a bias magnetic field $\boldsymbol{H}_B$ applied along the same direction and its magnitude

reduced in steps from 4000 to 500 Oe, with a full relaxation achieved at each step. In the second set of simulations, a spatially uniform alternating field $\boldsymbol{h}_{cw}$ of 1 Oe amplitude was applied along the *y*-axis:

$$\mathbf{h}_{cw} = \mathbf{h}_{cw,0}\sin\left(2\pi f \cdot t\right) \tag{1}$$

where *f* was the frequency of the excitation.

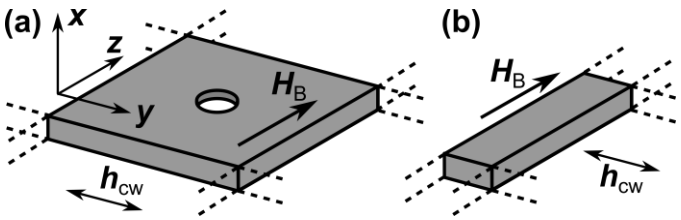

Fig. 1 (a) A circular antidot embedded within an otherwise continuous magnetic film is schematically shown. **(b)** A section of a very wide and infinitely long stripe (modeling a semi-infinite film) is schematically shown. Both samples are magnetized by a bias magnetic field $\boldsymbol{H}_B$, and the magnetization dynamics are excited by a time-varying field $\boldsymbol{h}_{cw}$.

III. Results & Discussion

(1) 40 nm thick antidot

Let us first consider the case of an antidot embedded within a 40 nm thick film. The spatial distribution of the projection of the static internal field $\boldsymbol{H}_i$ (the sum of the Zeeman $\boldsymbol{H}_B$ and demagnetizing $\boldsymbol{H}_{dem}$ fields) onto the static magnetization is shown in Fig. 2 (a), and strongly resembles that observed in Ref. [14]. Specifically, the regions above and below the antidot have a reduced internal field, and the regions immediately left and right of the antidot have an increased internal field (relative to the rest of the film where $\boldsymbol{H}_i \approx 500$ Oe). Due to the greater magnetization of saturation of Permalloy (as compared to that of YIG), the variation of the internal field across the sample here is substantially greater.

Using the internal field distribution presented in Fig. 2 (a), we can calculate the distribution of the "local FMR frequency" (f_{FMR}). This is defined as the limiting case of the spin-wave frequency as $k \to 0$, and in a continuous film [19] is given by the Kittel formula

$$f_{FMR} = \frac{\gamma}{2\pi}\sqrt{H_i\left(H_i + 4\pi M_S\right)} \tag{2}$$

Following the method from Ref. [14], Fig. 2 (b) shows the spatial variation of local resonance frequency $f_{FMR}(y,z)$, which is equal to 6.44 GHz in the continuous film. As expected, $f_{FMR}(y,z)$ resembles the distribution of $\boldsymbol{H}_i$ shown in Fig. 2 (a), in that low-frequency resonances exist above and below the antidot, and regions of high local FMR frequency sit left and right of the antidot. Now, a continuous excitation of the sample with a harmonic field transfers its energy most efficiently to the regions with similar local resonance frequency. E.g., exciting the entire system at a frequency of 9 GHz leads to the resonant excitation of ring-shaped regions with the local resonance frequency is equal to 9 GHz, which are located both the left and right sides of the antidot.

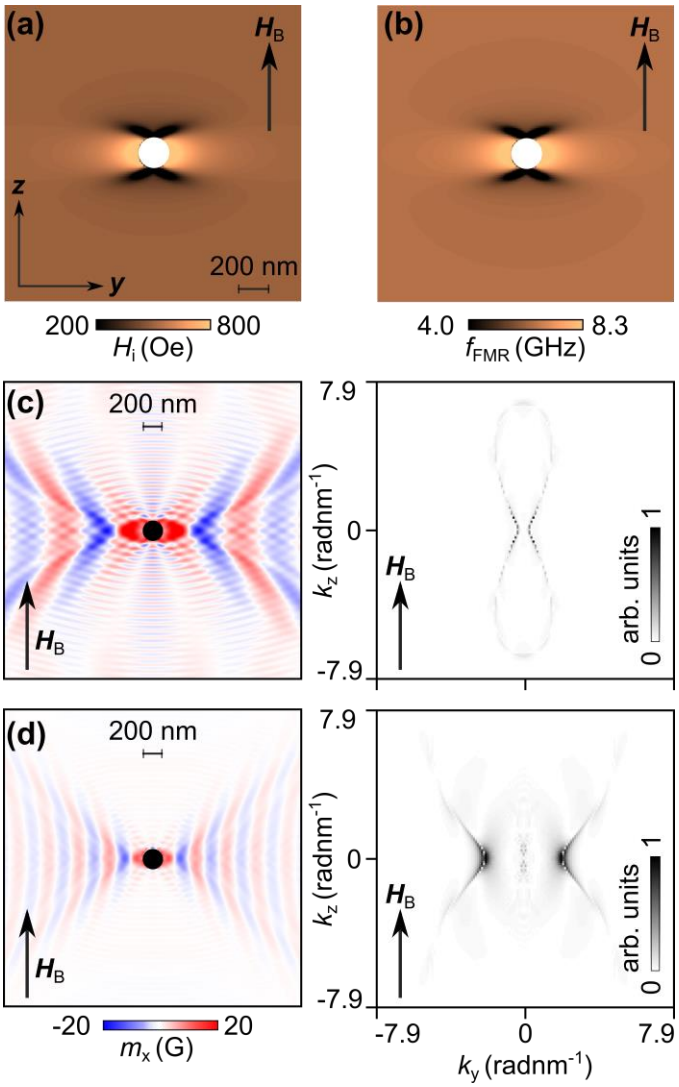

Fig. 2 (a) The calculated distribution of the internal field $\boldsymbol{H}_i$ onto the static magnetization in the vicinity of the antidot is shown. **(b)** The spatial variation of the local resonance frequency f_{FMR} corresponding to (a) is shown. **(c)-(d)** The calculated dynamic out-of-plane component of the magnetization 4 ns after the onset of the harmonic excitation (left panel) and the corresponding distribution of the spin wave amplitude in the reciprocal space (right panel) are shown for the 40 nm antidot sample excited at 9.0 GHz and 15.0 GHz frequency, respectively.

The result of exciting the sample at 9 GHz and 15 GHz is shown in the left panels of Figs. 2 (c) and (d). Shown here are snapshots of the dynamic out-of-plane component of magnetization taken 4 ns after the onset of the $\boldsymbol{h}_{cw}$ field. Generally, the directions of the phase and group velocities of the emitted spin waves are observed to form rather large angles. This is explained by the shape of the isofrequency curves characterizing the spin waves at the excitation frequency in reciprocal space (right panels of Figs. 2 (c) and (d), note the dc contribution has been nulled). The spin-wave

amplitude is predominantly concentrated across the small wave-vector, quasi-linear sections of the isofrequency curve [12], which leads to the non-collinear phase and group velocities and also 'beaming' of the spin wave amplitude.

(2) 6 nm thick antidot

Upon reducing the film thickness from 40 nm to 6 nm, it is anticipated that the exchange interaction will play a more significant role in the dispersion of the emitted spin waves. Shown in the left panel of Fig. 3 (a) is a snapshot of the dynamic out-of-plane component of the magnetization taken 4 ns after the onset of the pumping field of exciting field of 9 GHz frequency. In contrast to Fig. 2 (c), here the shape of the spin-wave phase fronts is determined by the shape of the source, propagating almost in a 'beam' like fashion, as also observed e.g. in Ref. [21]. This markedly different behavior arises due to the dominance of the exchange interaction and associated greater isotropy of the spin-wave dispersion, as one can see from the right panels of Fig. 3. Specifically, the exchange interaction has caused the isofrequency curves to become more elliptical in shape. With most of the excited spin-wave amplitude concentrated along the *y*-axis, the spin waves consequently have approximately parallel group and phase velocities. The dominance of the exchange interaction is more apparent at the higher excitation frequency of 15 GHz.

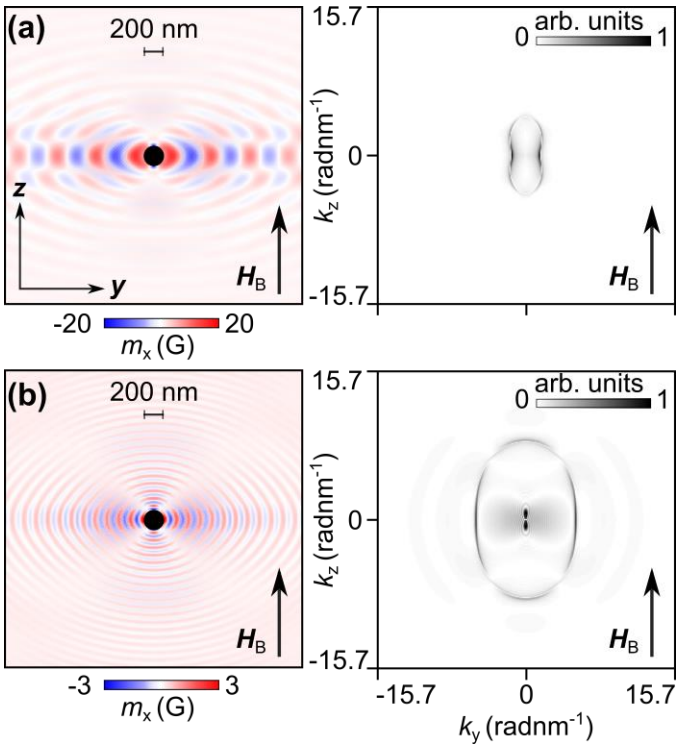

Fig. 3 (a)-(b) The calculated dynamic out-of-plane component of the magnetization taken about 4 ns after initial excitation (left panel) and the corresponding distribution of the spin-wave amplitude in reciprocal space (right panel) are shown for the 6 nm antidot sample excited at 9.0 GHz and 15.0 GHz frequency, respectively.

(3) Semi-infinite film

In the previous sections, the increase in the local FMR frequency was delivered through a combination of both the static and dynamic demagnetizing fields. Let us now consider spin-wave emission from an isolated straight edge of a semi-infinite magnetic film, modeled by a sufficiently wide magnetic stripe of infinite length (Fig. 1 (b)). The length, width and thickness of the stripe's supercell were 100 nm, 20 μm and 40 nm, respectively, and one-dimensional periodic boundary conditions [22] were applied along the *z*-axis (length direction) so as to form an infinitely long stripe. The stripe was magnetized along its long axis.

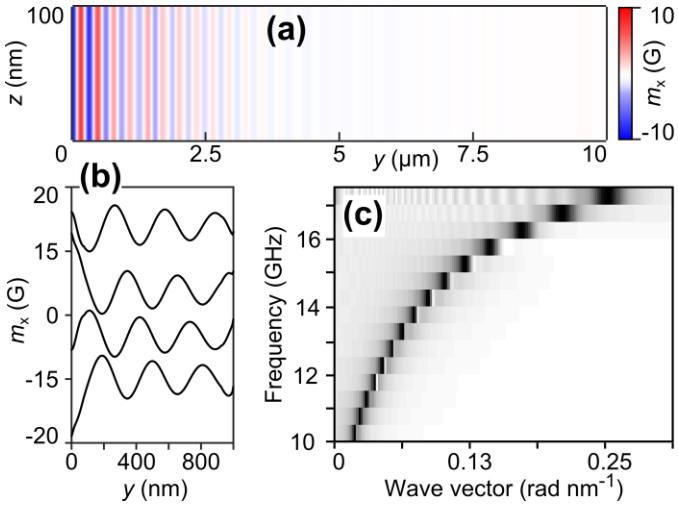

Fig. 4 (a) The calculated dynamic out-of-plane component of the magnetization across the first 10 μm from the film's edge, taken 4 ns after the onset of the excitation at 15 GHz frequency is shown. **(b)** Instantaneous profiles of the out-of-plane component of magnetization close to the film edge are shown for time intervals of 16.7 ps. **(c)** The dispersion relation of the emitted spin waves calculated from simulations performed using different excitation frequencies is shown.

The distribution of the static demagnetizing field across the width of the stripe is uniformly zero. In contrast, the dynamic demagnetizing field (i.e. the field induced by the magnetization precession leading to formation of dynamic magnetic charges at the film edge) is significantly non-uniform, highest at the film edge, and quickly decreasing as we move away from the edge. Hence, this sample allows us to verify if the dynamic demagnetizing field on its own could provide us with a source of propagating spin waves.

Presented in Fig. 4 (a) is the dynamic out-of-plane component of magnetization across the first 10 μm from the film's edge, extracted 4 ns after the onset of the excitation at 15 GHz. No quantized (standing) modes are observed, due to the film's width far exceeding being the spin-wave relaxation length (this indicates that the stripe models a semi-infinite film well). However, an oscillatory pattern of the dynamic magnetization is observed close to the film's edge instead. Sequential snapshots of the dynamic magnetization within the first micron from the edge are shown in Fig. 4 (b) in time steps of 16.7 ps. The snapshots reveal a propagating character of

the oscillations, confirming that we are indeed observing the emission of propagating spin waves.

To examine how the excited spin waves depend on the frequency of excitation, we repeated the dynamic simulations for a range of excitation frequencies from 10 to 17 GHz, in steps of 0.5 GHz. The spatial distributions of the wave field simulated at each frequency were Fourier transformed. Fig. 4 (c) shows the spin-wave dispersion calculated in this way, which resembles the Damon-Eshbach dispersion relation [23]. This reveals that the emitted spin waves are of the magneto-dipole nature (as expected from the thickness of the film).

The observed excitation of spin waves by the dynamic demagnetizing field could also be interpreted by noting that the field could be described by the effective pinning included within appropriate boundary conditions [24]. At the same time, the possibility of spin-wave excitation at boundaries with a finite pinning is well known [25-27] and is general indeed. The role of the dynamic demagnetizing field in generating the pinning can also be inferred from analytical calculations from Ref. 27, from which it follows that zero-pinning disables excitation of spin waves with a finite wave number in the exchange approximation.

IV. Conclusions

We have used micromagnetic simulations to demonstrate that propagating spin waves can be excited near edges of patterned nanostructures via targeted resonant excitation of well-defined regions of the nanostructures in which the static and / or dynamic internal magnetic field is raised compared to that far from the edges. This mechanism is capable of exciting both magneto-dipole and dipole-exchange spin waves, depending on the frequency of excitation and / or the film thickness. Furthermore, the uniformity of the exciting magnetic field implies that the excitation could also accompany such common measurement techniques of magnonics as cavity and waveguide based ferromagnetic resonance spectroscopy [28], time-resolved scanning Kerr microscopy [1] and microwave assisted Brillouin Light Scattering imaging [14],[20].

Acknowledgments

The research leading to these results has received funding from the Engineering and Physical Sciences Research Council (EPSRC) of the United Kingdom (Project Nos. EP/L019876/1 and EP/P505526/1).

References

[1] C. S. Davies *et al.*, "Towards graded-index magnonics: Steering spin waves in magnonic networks," *Phys. Rev. B* **92**, 020408(R) (2015).
[2] A. V. Sadovnikov *et al.*, "Magnonic beam splitter: The building block of parallel magnonic circuitry," *Appl. Phys. Lett.* **106**, 192406 (2015).
[3] M. Dvornik, Y. Au, and V. V. Kruglyak, "Micromagnetic simulations in magnonics," *Top. Appl. Phys.* **125**, 101 (2013).
[4] M. Krawczyk and D. Grundler, "Review and prospects of magnonic crystals and devices with reprogrammable band structure," *J. Phys.: Condens. Matter* **26**, 123202 (2014).
[5] S. Tacchi *et al.*, "Mode conversion from quantized to propagating spin waves in a rhombic antidot lattice supporting spin wave nanochannels," *Phys. Rev. B* **86**, 014417 (2012).
[6] C. Mathieu *et al.*, "Lateral quantization of Spin Waves in Micron Size Magnetic Wires," *Phys. Rev. Lett.* **81**, 3968 (1998).
[7] V. E. Demidov, M. P. Kostylev, K. Rott, J. Münchenberger, G. Reiss, and S. O. Demokritov, "Excitation of short-wavelength spin waves in magnonic waveguides," *Appl. Phys. Lett.* **99**, 082507 (2011).
[8] S. V. Vasiliev, V. V. Kruglyak, M. L. Sokolovskii, and A. N. Kuchko, "Spin wave interferometer employing a local nonuniformity of the effective magnetic field," *J. Appl. Phys.* **101**, 113919 (2007).
[9] K.-S. Lee and S.-K. Kim, "Conceptual design of spin wave logic gates based on a Mach-Zehnder-type spin wave interferometer for universal logic functions," *J. Appl. Phys.* **104**, 053909 (2008).
[10] J. Ding, M. Kostylev, and A. O. Adeyeye, "Realization of a mesoscopic reprogrammable magnetic logic based on a nanoscale reconfigurable magnonic crystal," *Appl. Phys. Lett.* **100**, 073114 (2012).
[11] S. A. Nikitov *et al*, "Magnonics: a new research area in spintronics and spin wave electronics," *Phys. Uspekhi* **58**, 1002 (2015).
[12] C. S. Davies *et al.*, "Field-Controlled Phase-Rectified Magnonic Multiplexer," *IEEE Trans. Magn.* **51**, 3401904 (2015).
[13] International Technology Roadmap for Semiconductors (ITRS) 2013 edition: Emerging Research Devices. http://www.itrs.net/Links/2013ITRS/Summary2013.htm, accessed Oct. 26, 2015.
[14] C. S. Davies et al., "Generation of propagating spin waves from regions of increased dynamic demagnetizing field near magnetic antidots," *Appl. Phys. Lett.* **107**, 162401 (2015).
[15] E. Schlömann, "Generation of spin waves in nonuniform magnetic fields. I. Conversion of electromagnetic power into spinwave power and vice versa," *J. Appl. Phys.* **35**, 159 (1964).
[16] V. Veerakumar and R. E. Camley, "Magnon focusing in thin ferromagnetic films," *Phys. Rev. B* **74**, 214401 (2009).
[17] M. Donahue and D. Porter, *Interagency Report NISTIR 6376* (NIST, Gaithersburg, MD, 1999).
[18] W. Wang *et al.*, "Two-dimensional periodic boundary conditions for demagnetization interactions in micromagnetics," *Comput. Mater. Sci.* **49**, 84 (2010).
[19] C. Kittel, "On the theory of spin waves in ferromagnetic media," *J. Phys. Radiat.* **12**, 291 (1951).
[20] R. Geniusz *et al.*, "Single antidot as a passive way to create caustic spin-wave beams in yttrium iron garnet films," *Appl. Phys. Lett.* **102**, 102409 (2013).
[21] P. Gruszecki, A. E. Serebryannikov, W. Śmigaj, and M. Krawczyk, "Microwave excitation of spin wave beams in thin ferromagnetic films," arXiv:1509.05061
[22] K. M. Lebecki, M. J. Donahue, and M. W. Gutowski, "Periodic boundary conditions for demagnetization interactions in micromagnetic simulations," J. Phys. D.: Appl. Phys. **41**, 175005 (2008).
[23] R. W. Damon and J. R. Eshbach, "Magnetostatic modes of a ferromagnet slab," *J. Phys. Chem. Solids* **19**, 308 (1961).
[24] K. Y. Guslienko, S. O. Demokritov, B. Hillebrands, and A. N. Slavin, "Effective dipolar boundary conditions for dynamic magnetization in thin magnetic stripes", *Phys. Rev. B* 66, 132402 (2002).
[25] C. Kittel, "Excitation of Spin Waves in a Ferromagnet by a Uniform rf Field", *Phys. Rev.* **110**, 1295 (1958).
[26] H. Puszkarski, "Theory of surface states in spin wave resonance", *Progr. Surf. Sci.* **9**, 191 (1979).
[27] R. V. Mikhaylovskiy, E. Hendry, and V. V. Kruglyak, "Negative permeability due to exchange spin-wave resonances in thin magnetic films with surface pinning", *Phys. Rev. B* **82**, 195446 (2010).
[28] O. N. Martyanov *et al.*, "Ferromagnetic resonance study of thin film antidot arrays: Experiment and micromagnetic simulations," *Phys. Rev. B* **75**, 174429 (2007).